Active Power Oscillation Cancelation With Peak Current Sharing in Parallel Interfacing Converters Under Unbalanced Voltage

Farzam Nejabatkhah, *Student Member, IEEE*, Yun Wei Li, *Senior Member, IEEE*, Kai Sun, *Senior Member, IEEE*, and Ruixue Zhang

***Abstract*—In a hybrid ac/dc grid, the ac-side unbalance voltage introduces adverse effects on dc grids and interfacing converters (IFC) (active power oscillations, dc-link voltage oscillations, and IFC peak current increase at the same average power production). For parallel IFCs, these adverse effects can be easily aggregated. In this paper, two new control strategies are proposed for parallel IFCs to improve both ac and dc subgrids power quality. The proposed control strategies focus on canceling active power oscillations of parallel IFCs that provide oscillation-free dc link and sharing collective peak current of parallel IFCs. In the first proposed control strategy, IFCs' power coefficients are controlled by solving a set of nonlinear equations, and this method is called as coefficient-based strategy, whereas, in the second proposed control strategy, peak currents of IFCs are controlled directly through the derived relationship of IFCs' peak currents under zero power oscillation in this paper, and this method is named as peak current based strategy. This peak current based strategy features much simplified calculation and could be easy to implement. To achieve control objectives, thorough study on parallel IFCs' peak currents is conducted. Based on the study, it is shown that the collective peak current of all IFCs is a constant under zero total active power oscillation, and therefore, keeping all IFCs' peak currents in the same phase and in-phase with collective peak current optimizes the utilization range of parallel IFCs. The numerical examples and experimental results are provided to verify the validity of the proposed control strategies under different operating conditions.**

***Index Terms*—Hybrid ac/dc microgrid, parallel interfacing converters (IFCs), peak current sharing, power/current transferring capability, power oscillations, secondary control, unbalanced voltage.**

I. Introduction

THE next generation of power systems are evolving to hybrid ac/dc microgrids, where ac/dc power generations and loads are integrated in a unified structure. In such systems, an ac-side unbalanced voltage is an important power quality concern that causes adverse effects on the power system and equipment [1]–[4]. Power electronics interfacing converters (IFCs) connecting ac–dc subgrids in hybrid ac/dc microgrids are affected by unbalanced voltage. The unbalanced voltage increases the IFCs' peak currents and reduces its power/current transferring capability. The unbalanced voltage causes double-frequency power oscillations at the output of IFCs, which are reflected in the dc-link voltage as ripples and harmonics (high-order harmonics can be easily filtered; however, second-order harmonics produce oscillation in dc side). The IFCs connecting ac–dc subgrids prefer to have a parallel structure to provide higher capacity, reliability, modularity, and efficiency (where some parallel units can be offline when power flow is low). In this case, the adverse effects of unbalance voltage on the power quality of both ac and dc sides can be aggregated. In parallel IFCs under unbalanced voltage, dc voltage oscillations affect the performance of systems connected to a dc subgrid, e.g., the maximum power point tracking (MPPT) of the photovoltaic (PV) converters connected to the dc subgrid [5]–[7]. These dc-side oscillations can be suppressed by dc–dc power converters in the dc subgrid; however, it will be desirable if dc–ac IFCs can be controlled properly to block transferring these oscillations to the dc side without additional investment on passive or active filters.

Currently, different control strategies have been proposed for a single IFC's operation under unbalanced voltage where output peak current and power oscillations, and dc-link voltage oscillation have been addressed [8]–[16]. However, these control strategies cannot guarantee reduction/cancelation of the adverse effects for parallel IFCs and cannot provide their optimal operation, and coordination among IFCs is essential. For a parallel IFCs' operation under unbalanced voltage, limited research has been done, and they are mainly focusing on parallel IFCs without common dc link [17]–[25]. New control strategies for parallel IFCs operation with common dc and ac links under unbalanced voltage are proposed in [26]–[28]. These control strategies cancel out active power oscillations of parallel IFCs using one dedicated IFC (called redundant) with largest power rating, which ensures oscillation-free dc-link voltage. However, collective peak current of parallel IFCs

Manuscript received July 19, 2017; revised November 6, 2017 and December 22, 2017; accepted January 24, 2018. Date of publication February 8, 2018; date of current version September 28, 2018. This paper was presented in part at the IEEE Energy Conversion Congress and Exposition, Milwaukee, WI, USA, September 2016. Recommended for publication by Associate Editor S. ElMoursi. *(Corresponding author: Farzam Nejabatkhah.)*

F. Nejabatkhah and Y. W. Li are with the Department of Electrical and Computer Engineering, University of Alberta, Edmonton, AB T6G 2V4 Canada (e-mail: nejabatk@ualberta.ca; yunwei.li@ualberta.ca).

K. Sun and R. Zhang are with the Department of Electrical and Computer Engineering, Tsinghua University, Beijing 100084, China (e-mail: sun-kai@mail.tsinghua.edu.cn; 18238825306@163.com).

Color versions of one or more of the figures in this paper are available online at http://ieeexplore.ieee.org.

Digital Object Identifier 10.1109/TPEL.2018.2803770

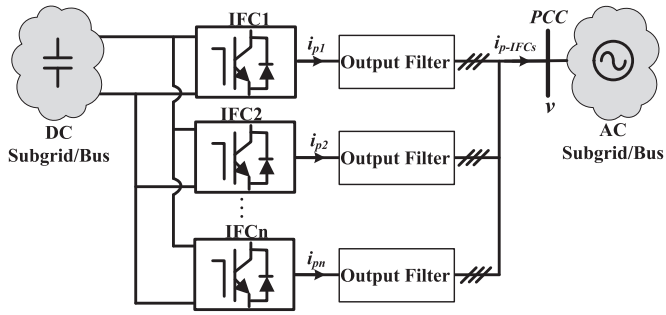

Fig. 1. Parallel IFCs with common dc and ac links under unity PF operation.

(which is a constant value under fixed average active and reactive powers as proved in this paper) is not shared among IFCs based on their power ratings. Therefore, some IFCs work under their current rating limits while the others operate far from their limits. Moreover, IFCs' peak current minimization (power/current transferring capability maximization) is not addressed. Also, the redundant converter power rating should be large enough to compensate other IFCs' power oscillation.

To address the above-mentioned current sharing concerns, two new control strategies for parallel IFCs' operation under unbalanced voltage are proposed in this paper. These control strategies are focusing on active power oscillation cancelation and parallel IFCs' collective peak current sharing among IFCs based on their power ratings, which provides the same available rooms for IFCs' operation. In addition, the power/current transferring capability of parallel IFCs is maximized. In this paper, thorough study on relationship between individual and parallel IFCs' peak currents with active power oscillation reveals that the collective peak current of parallel IFCs is a constant value under zero active power oscillations and fixed average active powers. Moreover, an individual IFCs' peak currents can be controlled to be in the same phase and in-phase with collective peak current of parallel IFCs, which provides minimum IFCs' peak currents' summation and maximizes the power/current transferring capability of parallel IFCs. The analysis in this paper and the two proposed control strategies are verified by experiments.

This paper is organized as follows. In Section II, instantaneous active and reactive powers of parallel IFCs under the unity power factor (PF) operation are studied, and a constraint in which the parallel IFCs' collective active power oscillation is zero is provided. The individual and parallel IFCs' peak currents analysis and the parallel IFCs' power/current transferring capability are addressed in Section III. In Section IV, the two proposed control strategies are provided. The experimental verifications are presented in Section V. Finally, Section VI summarizes this paper and lists conclusions.

II. Parallel Three-Phase IFCs Instantaneous Power Analysis

In Fig. 1, a typical *n*-parallel IFCs with common dc and ac links is shown. From instantaneous power theory principles [8], [29], the individual ith IFC's symmetric sequence based instantaneous active and reactive powers in unity PF operation can be derived as follows:

$$p_i = v\cdot i_{pi} = \left(v^+ + v^-\right)\cdot\left(i_{pi}^+ + i_{pi}^-\right) = \left(\underbrace{v^+\cdot i_{pi}^+}_{P_i^+} + \underbrace{v^-\cdot i_{pi}^-}_{P_i^-}\right) + \left(\underbrace{v^+\cdot i_{pi}^- + v^-\cdot i_{pi}^+}_{\Delta P_i}\right) = P_i + \Delta P_i \tag{1}$$

$$q_i = v_\perp\cdot i_{pi} = \left(v_\perp^+ + v_\perp^-\right)\cdot\left(i_{pi}^+ + i_{pi}^-\right) = \left(\underbrace{v_\perp^+\cdot i_{pi}^- + v_\perp^-\cdot i_{pi}^+}_{\Delta Q_i}\right) = \Delta Q_i \tag{2}$$

where $v = [\,v_a, v_b, v_c]$ and $i_{pi} = [i_{api}, i_{bpi}, i_{cpi}]$ are three-phase point of common coupling (PCC) voltage vector and the ith IFC's output current vector, $v_\perp$ lags v by 90°, $v^+, v^-, i_{pi}^+, i_{pi}^-$ are positive and negative sequence vectors of v and i_{pi}, P_i and ΔP_i are average and oscillatory terms of instantaneous active power, P_i^+ and P_i^- are the positive and negative sequence components of P_i, and ΔQ_i is the oscillatory term of instantaneous reactive power. In the equations, subscript "p" refers to unity PF operation mode. In this paper, it is assumed that the zero sequence of current does not exist. Moreover, system does not contain high-order harmonics and just fundamental components exist.

According to [26] and [27], ith IFC's active and reactive power oscillations under unity PF can be canceled out by using power coefficient k_{pi}. Thus, the ith IFC's reference current vector in unity PF operation is obtained as follows:

$$i_{pi}^* = i_{pi}^{+*} + i_{pi}^{-*} = \frac{P_i}{|v^+|^2 + k_{pi}|v^-|^2}\,v^+ + \frac{P_i k_{pi}}{|v^+|^2 + k_{pi}|v^-|^2}\,v^- \tag{3}$$

where superscript "$*$" refers to reference values, and $|v^+|$ and $|v^-|$ are the modules (also called norms or magnitudes) of positive and negative sequence vectors of v, respectively. In this paper, space vectors of the three-phase sinusoidal positive and negative sequence voltages (v^+ and v^-) are considered as $\overrightarrow{v^+} = |v^+|\ e^{j(\omega t+\theta^+)}$ and $\overrightarrow{v^-} = |v^-|\ e^{j(-\omega t+\theta^-)}$. Considering (3), individual ith IFC's instantaneous active and reactive powers can be achieved by using (1) and (2) as follows:

$$p_i = P_i + \Delta P_i = P_i + \frac{P_i\,(1+k_{pi})\,(v^+.\,v^-)}{|v^+|^2 + k_{pi}|v^-|^2} = P_i + \frac{P_i\,(1+k_{pi})}{|v^+|^2 + k_{pi}|v^-|^2}\,|v^+|\,|v^-|\cos(2\omega t + 2\rho) \tag{4}$$

$$q_i = \Delta Q_i = \frac{P_i\,(1-k_{pi})\,\left(v^+.\,v_\perp^-\right)}{|v^+|^2 + k_{pi}|v^-|^2} = \frac{P_i\,(1-k_{pi})}{|v^+|^2 + k_{pi}|v^-|^2}\,|v^+|\,|v^-|\sin(2\omega t + 2\rho) \tag{5}$$

where $\rho = (\theta^+ - \theta^-)/2$. From (3) to (5), it can be concluded that under unbalanced condition, the following statements hold:

1) individual IFC's output active and reactive powers oscillate at two times the grid frequency;
2) IFC's output current will increase in the fixed average active power output;
3) $k_{pi}=-1$ results in zero active power oscillation of ith IFC; and 4) $k_{pi}=0$ provides balanced output current of IFC.

For *n*-parallel IFCs with common dc and ac links, as shown in Fig. 1, the reference current vector and instantaneous active and reactive powers under unity PF can be achieved by using individual IFC's relations in (1)–(5)

$$i^*_{p-\mathrm{IFC}s}=\sum_{i=1}^{n} i^*_{pi}=\sum_{i=1}^{n}\frac{P_i}{|v^+|^2+k_{pi}|v^-|^2}v^+ +\sum_{i=1}^{n}\frac{P_i k_{pi}}{|v^+|^2+k_{pi}|v^-|^2}v^- \tag{6}$$

$$p=\sum_{i=1}^{n}P_i+\sum_{i=1}^{n}\frac{P_i\left(1+k_{pi}\right)\left(v^+.v^-\right)}{|v^+|^2+k_{pi}|v^-|^2} =\sum_{i=1}^{n}P_i+\sum_{i=1}^{n}\frac{P_i\left(1+k_{pi}\right)}{|v^+|^2+k_{pi}|v^-|^2} \times\left|v^+\right|\left|v^-\right|\cos\left(2\omega t+2\rho\right) \tag{7}$$

$$q=\sum_{i=1}^{n}\frac{P_i\left(1-k_{pi}\right)\left(v^+.v^-_{\perp}\right)}{|v^+|^2+k_{pi}|v^-|^2} =\sum_{i=1}^{n}\frac{P_i\left(1-k_{pi}\right)}{|v^+|^2+k_{pi}|v^-|^2}\left|v^+\right|\left|v^-\right|\sin\left(2\omega t+2\rho\right). \tag{8}$$

Considering (7), to cancel out *n*-parallel IFCs' active power oscillations, following constraint should be satisfied [26], [27]:

$$\sum_{i=1}^{n}\frac{P_i\left(1+k_{pi}\right)\left(v^+.v^-\right)}{|v^+|^2+k_{pi}|v^-|^2}=0\ \Rightarrow\ \sum_{i=1}^{n}\frac{P_i}{|v^+|^2+k_{pi}|v^-|^2} =\frac{\sum_{i=1}^{n}P_i}{|v^+|^2-|v^-|^2}\,. \tag{9}$$

By applying (9) into (6)–(8), the *n*-parallel IFCs reference current vector and instantaneous active and reactive powers under zero active power oscillations are obtained as follows:

$$i^*_{p-\mathrm{IFC}s}\big|_{\Delta P=0}=\left(\sum_{i=1}^{n}i^*_{pi}\right)\Bigg|_{\Delta P=0} =\left(\sum_{i=1}^{n}i^{+\,*}_{pi}+\sum_{i=1}^{n}i^{-\,*}_{pi}\right)\Bigg|_{\Delta P=0} =\frac{\sum_{i=1}^{n}P_i}{|v^+|^2-|v^-|^2}v^+ +\frac{-\sum_{i=1}^{n}P_i}{|v^+|^2-|v^-|^2}v^- \tag{10}$$

$$p=\sum_{i=1}^{n}P_i \tag{11}$$

$$q=\frac{2\left(v^+\cdot v^-_{\perp}\right)}{|v^+|^2-|v^-|^2}\sum_{i=1}^{n}P_i\,. \tag{12}$$

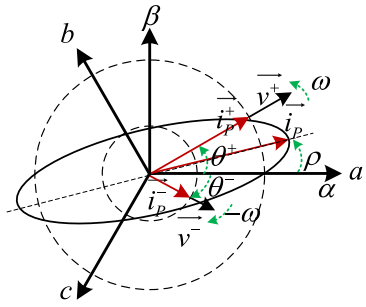

Fig. 2. Locus of the PCC voltage and the ith IFC reference current space vectors under unity PF operation.

Considering (10)–(12), the positive and negative sequence current as well as the reactive power oscillation of parallel IFCs are independent from k_{pi} under zero active power oscillations, and they are just affected by $\sum_{i=1}^{n}P_i$ variations.

III. Parallel IFCs Power/Current Transferring Capability

Here, power/current transferring capability of parallel IFCs is studied in detail. For that, thorough study on individual and parallel IFCs' peak currents under unbalanced voltage is conducted. Then, the conditions in which the power/current transferring capability of IFCs can be maximized are provided.

A. Peak Current Analysis of IFCs Under Unity PF Operation

For individual ith IFC under unity PF operation, considering reference current vector in (3) and assuming $\overrightarrow{v^+}=|v^+|\,e^{j(\omega t+\theta^+)}$, $\overrightarrow{v^-}=|v^-|\,e^{j(-\omega t+\theta^-)}$, and $\rho=(\theta^+-\theta^-)/2$, the locus of PCC positive and negative sequences voltage space vectors and the output reference current space vector are shown in Fig. 2. In this figure, the big and small dashed circles are the locus of positive and negative sequences reference current space vectors, and the ellipse is the locus of the total reference current space vector.

Considering reference current ellipse in Fig. 2, the maximum current at each phase of the individual ith IFC is the maximum projection of that ellipse on the abc axis [29]. Considering (3) and Fig. 2, the projection of reference current ellipse on the abc axis can be derived as follows:

$$i^{*\prime}_{xpi}=\Bigg(\underbrace{\frac{P_i\,|v^+|}{|v^+|^2+k_{pi}|v^-|^2}+\frac{P_i k_{pi}\,|v^-|}{|v^+|^2+k_{pi}|v^-|^2}}_{I_{pLi}}\Bigg)\cos\gamma\cos\left(\omega t\right) -\Bigg(\underbrace{\frac{P_i\,|v^+|}{|v^+|^2+k_{pi}|v^-|^2}-\frac{P_i k_{pi}\,|v^-|}{|v^+|^2+k_{pi}|v^-|^2}}_{I_{pSi}}\Bigg) \times\sin\gamma\sin\left(\omega t\right)\ \ x=a,b,c \tag{13}$$

where $i^{*\prime}_{xpi}$ is the value of reference current ellipse projection on the phase x, I_{pLi} and I_{pSi} are semimajor and semiminor axis lengths of ellipse, and γ is rotation angle, which is equal to ρ, $\rho+\pi/3$, and $\rho-\pi/3$ for *abc* axis, respectively. From (13), for individual ith IFC, maximum current in each phase, the peak current, and the phase angle of peak current under unity PF can be derived [27] (14) as shown at the bottom of this page.

$$I_{pi}^{\max} = \max\left(I_{api}^{\max}, I_{bpi}^{\max}, I_{cpi}^{\max}\right) \tag{15}$$

$$\delta_i|_{I_{pi}^{\max}} = \tan^{-1}\left(\cot\gamma\left(-1-\frac{2k_{pi}\,|v^-|}{|v^+|-k_{pi}\,|v^-|}\right)\right). \tag{16}$$

From (14) to (16), the individual IFC's maximum current at each phase and its peak current amplitude and phase angle depend on power coefficient (k_{pi}) and the PCC voltage components. In a simulated case study in Fig. 3, it is shown that how different values of k_{pi} affect the maximum current at each phase and the peak current of individual IFC under different phase angles ρ and average active power output. As seen from this figure, different values of k_{pi} and ρ lead peak current to different phases, which will be discussed in more detail.

For *n*-parallel IFCs with unity PF operation under zero active power oscillations, the projection of collective reference current ellipse on *abc* axis can be achieved using (10) and (13) as follows:

$$i^{*\prime}_{xp-\mathrm{IFCs}}\big|_{\Delta P=0} = \underbrace{\left(\frac{|v^+|\sum_{i=1}^{n}P_i}{|v^+|^2-|v^-|^2}-\frac{|v^-|\sum_{i=1}^{n}P_i}{|v^+|^2-|v^-|^2}\right)}_{I_{pL-\mathrm{IFCs}}|_{\Delta P=0}}\cos\gamma\,\cos(\omega t)$$
$$-\underbrace{\left(\frac{|v^+|\sum_{i=1}^{n}P_i}{|v^+|^2-|v^-|^2}+\frac{|v^-|\sum_{i=1}^{n}P_i}{|v^+|^2-|v^-|^2}\right)}_{I_{pS-\mathrm{IFCs}}|_{\Delta P=0}}$$
$$\times\sin\gamma\sin(\omega t)\qquad x=a,b,c. \tag{17}$$

From (17), the collective maximum current in each phase, and the collective peak current and its phase angle can be obtained as (18) as shown at the bottom of this page.

$$I_{p-\mathrm{IFCs}}^{\max}\big|_{\Delta P=0} = \max\left(I_{ap-\mathrm{IFCs}}^{\max}\big|_{\Delta P=0}, I_{bp-\mathrm{IFCs}}^{\max}\big|_{\Delta P=0}, I_{cp-\mathrm{IFCs}}^{\max}\big|_{\Delta P=0}\right) \tag{19}$$

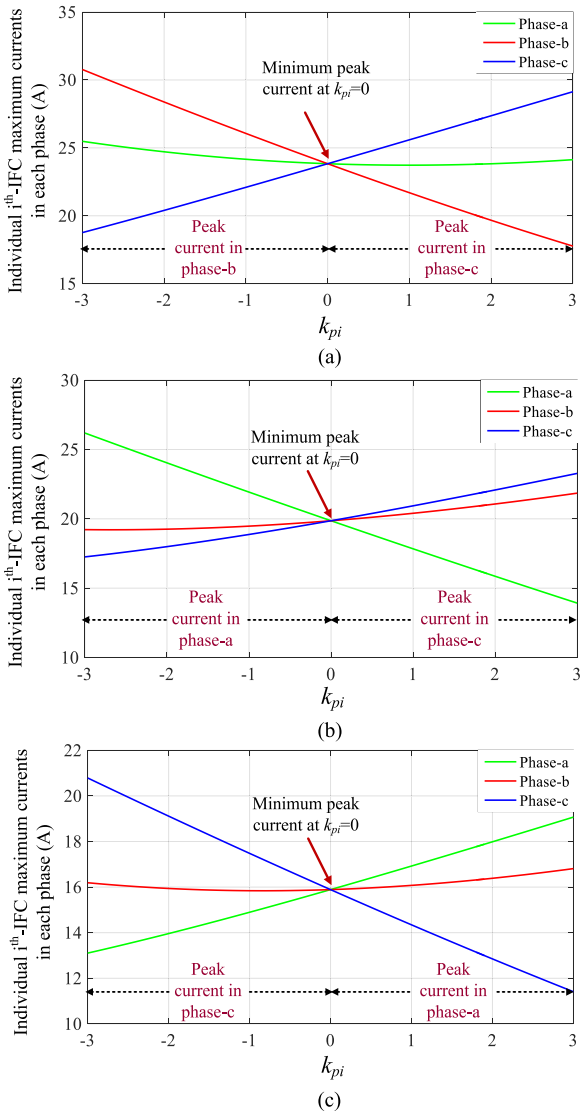

Fig. 3. Individual ith IFC's maximum currents in each phase under different k_{pi}, phase angle (ρ), and average active powers ($|v^+|=168\,\mathrm{V}$, $|v^-|=16\,\mathrm{V}$): (a) $\rho=45$, $P_i=6\,\mathrm{kW}$; (b) $\rho=85$, $P_i=5\,\mathrm{kW}$; and (c) $\rho=160$, $P_i=4\,\mathrm{kW}$.

$$\delta|_{I_{p-\mathrm{IFCs}}^{\max}}\big|_{\Delta P=0} = \tan^{-1}\left(\cot\gamma\left(-1+\frac{2\,|v^-|}{|v^+|+|v^-|}\right)\right). \tag{20}$$

From (18) to (20), the parallel IFCs' collective peak current amplitude and phase angle under $\Delta P=0$ are independent from k_{Pi}, and they are constant values with fixed active power output.

$$I_{xpi}^{\max} = \sqrt{\left(\frac{P_i}{|v^+|^2+k_{pi}|v^-|^2}\right)^2\times\left(|v^+|^2+|v^-|^2k_{pi}^2+2\,|v^+|\,|v^-|\,k_{pi}\cos(2\gamma)\right)}\qquad x=a,b,c \tag{14}$$

$$I_{xp-\mathrm{IFCs}}^{\max}\big|_{\Delta P=0} = \sqrt{\left(\frac{\sum_{i=1}^{n}P_i}{|v^+|^2-|v^-|^2}\right)^2\times\left(|v^+|^2+|v^-|^2-2\,|v^+|\,|v^-|\cos(2\gamma)\right)}\qquad x=a,b,c \tag{18}$$

B. Maximizing Power/Current Transferring Capability of Parallel IFCs

As mentioned, under the unbalance condition, IFCs' output peak currents increase and active power oscillation cancelation may worsen this situation. As a result, power/current transferring capability of IFCs reduces. Here, it is studied that how the power/current transferring capability of parallel IFCs is maximized (in other words, how to minimize the summation of individual IFCs' peak currents).

1) IFCs Operation Under Various PFs: In general, for n-parallel IFCs under various PFs and zero collective active power oscillation, three-phase current phasors based on maximum currents can be represented as follows:

$$\begin{aligned}
&\sum_{i=1}^{n} I_{ai}^{\max}\angle\delta_{ai}|_{I_{ai}^{\max}} = I_{a-\mathrm{IFCs}}^{\max}\big|_{\Delta P=0}\ \angle\delta_a|_{I_{a-\mathrm{IFCs}}^{\max}|_{\Delta P=0}}\\
&\sum_{i=1}^{n} I_{bi}^{\max}\angle\delta_{bi}|_{I_{bi}^{\max}} = I_{b-\mathrm{IFCs}}^{\max}\big|_{\Delta P=0}\ \angle\delta_b|_{I_{b-\mathrm{IFCs}}^{\max}|_{\Delta P=0}}\\
&\sum_{i=1}^{n} I_{ci}^{\max}\angle\delta_{ci}|_{I_{ci}^{\max}} = I_{c-\mathrm{IFCs}}^{\max}\big|_{\Delta P=0}\ \angle\delta_c|_{I_{c-\mathrm{IFCs}}^{\max}|_{\Delta P=0}}.
\end{aligned} \tag{21}$$

In (21), subscript "p" is not used since IFCs under different PFs are considered. It is worth mentioning again that $I_{x-\mathrm{IFCs}}^{\max}|_{\Delta P=0}$ and $\delta_x|_{I_{x-\mathrm{IFCs}}^{\max}|_{\Delta P=0}}$ (amplitude and phase angle of collective maximum current of parallel IFCs in phase x under $\Delta P=0$) are constant values. Assuming that the phase angles of individual IFCs' maximum currents in each phase are equalized with the phase angle of collective maximum current of parallel IFCs in that phase ($\angle\ \delta_{x1}|_{I_{x1}^{\max}} = \angle\ \delta_{x2}|_{I_{x2}^{\max}} = \cdots = \delta_{xn}|_{I_{xn}^{\max}} = \angle\delta_x|_{I_{x-\mathrm{IFCs}}^{\max}|_{\Delta P=0}}; x=a,b,c$), (21) can be rewritten as follows:

$$\begin{aligned}
&I_{a1}^{\max'} + I_{a2}^{\max'} + \cdots + I_{an}^{\max'} = \sum_{i=1}^{n} I_{ai}^{\max'} = I_{a-\mathrm{IFCs}}^{\max}\big|_{\Delta P=0}\\
&I_{b1}^{\max'} + I_{b2}^{\max'} + \cdots + I_{bn}^{\max'} = \sum_{i=1}^{n} I_{bi}^{\max'} = I_{b-\mathrm{IFCs}}^{\max}\big|_{\Delta P=0}\\
&I_{c1}^{\max'} + I_{c2}^{\max'} + \cdots + I_{cn}^{\max'} = \sum_{i=1}^{n} I_{ci}^{\max'} = I_{c-\mathrm{IFCs}}^{\max}\big|_{\Delta P=0}
\end{aligned} \tag{22}$$

where superscript "$'$" refers to maximum currents values after phases equalization. From (22), although phase angles equalization can reduce the summation of individual IFCs maximum currents in each phase ($\sum_{i=1}^{n} I_{xi}^{\max'} \le \sum_{i=1}^{n} I_{xi}^{\max};\quad x=a,b,c$), it cannot guarantee to minimize the summation of individual IFCs' peak currents without considering the phases that the peak currents are in. In more detail, if it is assumed that m numbers of IFCs' peak currents are in the phase a, u numbers are in the phase b, and $n-m-u$ numbers are in the phase c ($n \ge m+u$), following expression will be obtained:

$$\begin{aligned}
&\sum_{i=1}^{m} I_{ai}^{\max'} + \sum_{i=m+1}^{m+u} I_{bi}^{\max'} + \sum_{i=m+u+1}^{n} I_{ci}^{\max'} > I_{a-\mathrm{IFCs}}^{\max}\big|_{\Delta P=0}\\
&\sum_{i=1}^{m} I_{ai}^{\max'} + \sum_{i=m+1}^{m+u} I_{bi}^{\max'} + \sum_{i=m+u+1}^{n} I_{ci}^{\max'} > I_{b-\mathrm{IFCs}}^{\max}\big|_{\Delta P=0}\\
&\sum_{i=1}^{m} I_{ai}^{\max'} + \sum_{i=m+1}^{m+u} I_{bi}^{\max'} + \sum_{i=m+u+1}^{n} I_{ci}^{\max'} > I_{c-\mathrm{IFCs}}^{\max}\big|_{\Delta P=0}.
\end{aligned} \tag{23}$$

Therefore, from (23), it is seen that to minimize the summation of individual IFCs' peak currents ($\min\ (\sum_{i=1}^{n} I_i^{\max}) = I_{\mathrm{IFCs}}^{\max}|_{\Delta P=0}$), or in other words, to maximize the parallel IFCs power/current transferring capability, all individual IFCs' peak currents should be kept in the same phase and in-phase with parallel IFCs' collective peak current. This is a general conclusion independent from the unbalanced voltage level and IFCs average output active powers, and can be used for parallel IFCs operating under different PFs. For example, two-parallel IFCs with nonunity PF operations with the average active and reactive powers of $P_1 = 4$ kW, $P_2 = 5$ kW, $Q_1 = 7$ kvar, and $Q_2 = 0.5$ kvar are considered here. In this system, in case that $k_{p1} = -0.7$, $k_{q1} = 0.76$, $k_{p2} = -1.3$, and $k_{q2} = 6.2$ (k_{qi} are used to control active power oscillations associated with the average reactive powers [10]), the collective active power oscillation is zero ($\Delta P = 0$), and all the peak currents are in phase b and in-phase with the value of $I_{p-\mathrm{IFCs}}^{\max}|_{\Delta P=0} = 49$, $I_{pi}^{\max} = 27.2$ A, and $I_{pi}^{\max} = 21.5$ A ($I_{p-\mathrm{IFCs}}^{\max}\big|_{\Delta P=0} \approx I_{p1}^{\max} + I_{p2}^{\max}$). However, in case that $k_{p1} = -1.81$, $k_{q1} = -1.39$, $k_{p2} = -0.24$, and $k_{q2} = -15.85$, although collective active power oscillation is zero again, the peak current of the first, second, and collective peak current are in phase c, a, and b, respectively, with the value of $I_{p-\mathrm{IFCs}}^{\max}|_{\Delta P=0} = 49.01$, $I_{pi}^{\max} = 42.05$ A, and $I_{pi}^{\max} = 33.36$ A ($I_{p-\mathrm{IFCs}}^{\max}\big|_{\Delta P=0} \ll I_{p1}^{\max} + I_{p2}^{\max}$).

It should also be highlighted that, here, summation of n-parallel IFCs' peak currents are minimized to maximize parallel IFCs power/current transferring capability, and the individual IFCs' peak current values are not addressed directly. Although in most cases, individual IFCs' peak currents are reduced by this strategy, the distribution of peak current among parallel IFCs is not controlled. Considering this issue, in both proposed control strategies, individual IFCs' peak currents will be adjusted based on their power ratings. As a result, not only parallel IFCs power/current transferring capability is maximized, but also individual IFCs operation is optimized.

2) IFCs Operation Under Unity PFs: Under unity PF operation, from (16) and (20), the phase angles of individual IFCs maximum currents in each phase depend on k_{pi}, whereas in parallel IFCs under $\Delta P = 0$, the phase angles of collective maximum currents in each phase are independent from k_{pi}. However, since in parallel IFCs with common dc and ac links, $|v^+|$, $|v^-|$, and γ are common values in individual and parallel IFCs, and the variations of $\delta_{xi}|_{I_{xpi}^{\max}}$ (when k_{pi} deviates from $k_{pi} = -1$) are small enough (under $k_{pi} = -1$,

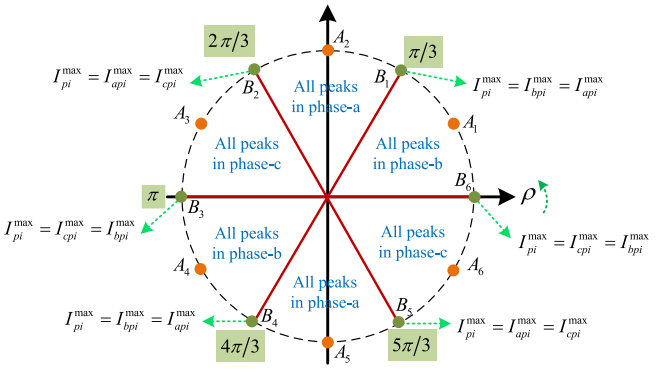

Fig. 4. Phase that all the peak currents (IFCs' peak currents and parallel IFCs collective peak current) are in that phase under different values of ρ when $k_{pi}<0;\ i=1,\ldots,n$.

$\delta_{xi}|_{I_{xpi}^{\max}}=\delta_x|_{I_{xp-\mathrm{IFCs}}^{\max}|_{\Delta P=0}};\quad x=a,b,c)$, the $\delta_{xi}|_{I_{xpi}^{\max}}$ in each phase can be assumed constant under k_{pi} variations and equal to $\delta_x|_{I_{xp-\mathrm{IFCs}}^{\max}|_{\Delta P=0}}$ with a good approximation. For more investigation, the variation of $\delta_{xi}|_{I_{\mathrm{xpi}}^{\max}}$ with respect to k_{pi} deviation are derived as in (24) by using (16)

$$\Delta\delta_{xi}|_{I_{xpi}^{\max}} = \frac{-2\,|v^+|\,|v^-|\cot\gamma}{\left(|v^+|-k_{pio}\,|v^-|\right)^2+(\cot\gamma)^2\times\left(|v^+|+k_{pio}\,|v^-|\right)^2}\,\Delta k_{pi} \qquad x=a,b,c \tag{24}$$

where k_{pio} is the initial operation point which is -1 in this case. From (24), it can be understood that $\Delta\delta_{xi}|_{I_{xpi}^{\max}}$ over Δk_{Pi} is small value in each phase. As a numerical example, in three-parallel IFCs with $P_1=6$ kW, $P_2=2$ kW, $P_3=3.6$ kW, $k_{pio}=-1$, $p=55°$, $|v^+|=168$ V, and $|v^-|=16$ V, the deviation of $\delta_{xi}|_{I_{xpi}^{\max}}$ in three abc phases from its initial point (where $k_{pi}=-1$ and $\delta_{xi}|_{I_{xpi}^{\max}}=\delta_x|_{I_{xp-\mathrm{IFCs}}^{\max}|_{\Delta P=0}};\quad x=a,b,c$) under $\Delta k_{pi}=2$ are $\Delta\delta_{ai}|_{I_{api}^{\max}}\approx 8°$, $\Delta\delta_{bi}|_{I_{\mathrm{bpi}}^{\max}}\approx 6°$, and $\Delta\delta_{ci}|_{I_{\mathrm{cpi}}^{\max}}\approx 2°$. Therefore, it can be concluded that $\delta_{xi}|_{I_{xpi}^{\max}}\approx\delta_x|_{I_{xp-\mathrm{IFCs}}^{\max}|_{\Delta P=0}};\quad x=a,b,c$ in the range of k_{pi} operation with a good approximation.

On the other hand, from (18), among three phases, the collective peak current of parallel IFCs is in the phase that $\cos(2\gamma)$ has its minimum value. For an individual ith IFC from (14), if $k_{pi}<0$, the peak current is in the phase in which $\cos(2\gamma)$ has its minimum value. Since keeping all IFCs' peak currents in the same phase with collective peak current of parallel IFCs is desired, all IFCs' k_{pi} will be kept less than zero ($k_{pi}<0$). As a result, regardless of ρ and active power flow direction, all IFCs' peak currents will be in the same phase with collective peak current of parallel IFCs (it is also proved above that they are approximately in phase). In Fig. 4, the phase that all the peak currents (IFCs' peak currents and parallel IFCs collective peak current) are in that phase under different values of ρ when $k_{pi}<0$ is shown. From Fig. 4 and considering Fig. 3 and (14), following conclusions are achieved.

1) The grid condition (the value of ρ) determines the phase that all the peak currents are in that phase.
2) When $\rho=i\pi/6\,(i=1,\ 3,\ 5,\ 7,\ 9,\ 11)$, individual IFCs' peak currents have their maximum possible values under determined k_{pi} since $\cos(2\gamma)=-1$ (see points $A_j(j=1,\ldots,6)$ in Fig. 4).
3) When ρ moves away from $\rho=i\pi/6\ (i=1,\ 3,\ 5,\ 7,\ 9,\ 11)$ toward boundaries where $\rho=i\pi/3\ (i=1,\ 2,\ \ldots,6)$, individual IFCs' peak currents will reduce from their maximum possible values.
4) When $\rho=i\pi/3\ (i=1,\ 2,\ldots,6)$, individual IFCs' peak currents have their minimum possible values under determined $k_{pi}(\cos(2\gamma)=-0.5)$. In these points, individual IFCs' peak currents will be equal to their one of other phases' maximum currents (see points $B_j(j=1,\ldots,6)$ in Fig. 4).

With the aforementioned discussions, under $k_{pi}<0;\quad i=1,\ldots,n$ and unity PF operation of IFCs, following relation among peak currents of individual IFCs and collective peak current of parallel IFCs with unity PF operations could be derived:

$$I_{p-\mathrm{IFCs}}^{\max}\cong\sum_{i=1}^{n}I_{pi}^{\max}. \tag{25}$$

From (25), it is concluded that the collective peak current of n-parallel IFCs, which is a constant value under zero collective active power oscillation and fixed output active powers, can be shared linearly among individual IFCs.

IV. Proposed Control Strategies for Parallel IFCs Operation Under Unbalanced Voltage: Active Power Oscillation Cancelation With Peak Current Sharing

Two control strategies are proposed for parallel IFCs to reduce unbalanced voltage adverse effects on their operations, and improve both ac and dc subgrids power quality. In this paper, the proposed control strategies ensure zero collective active power oscillations of parallel IFCs, share the collective peak current among parallel IFCs based on their power ratings, and maximize the power/current transferring capability of n-parallel IFCs. In the following, the proposed control strategies are explained in detail.

A. Control Strategy-1: Coefficient-Based Control Strategy

In this control strategy, following expressions are considered to achieve the control objectives:

$$\sum_{i=1}^{n}\frac{P_i}{|v^+|^2+k_{p_i}|v^-|^2}=\frac{\sum_{i=1}^{n}P_i}{|v^+|^2-|v^-|^2} \tag{26}$$

$$U_1I_{p1}^{\max}=U_2I_{p2}^{\max}=\cdots=U_nI_{pn}^{\max} \tag{27}$$

$$U_i=\frac{S_1}{S_i}\quad i=1,\ 2,\ldots,n \tag{28}$$

$$k_{pi}\le 0\ i=1,\ 2,\ldots,n \tag{29}$$

where U_i, S_i, and $I_{pi}^{\max}$ are sharing factor, power rating, and peak current of the ith IFC, respectively. In (26), the $I_{pi}^{\max}$ is obtained using (14) and (15). Solving a set of nonlinear equations in (26)–(28) considering (29), k_{pi} of all IFCs are deter-

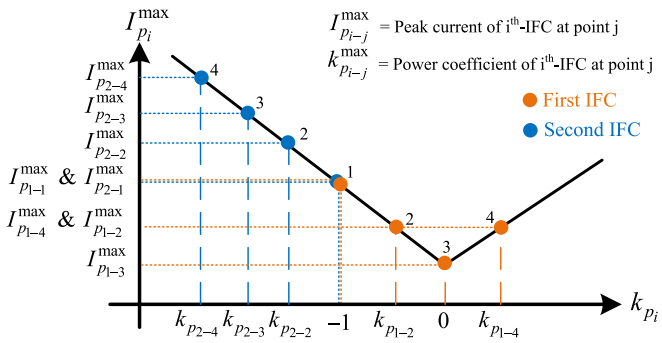

Fig. 5. Example for explaining the concept of the proposed control strategy; 2-parallel IFCs' peak currents relationships with k_{pi} under $P_1 = P_2$ and $S_1 < S_2$.

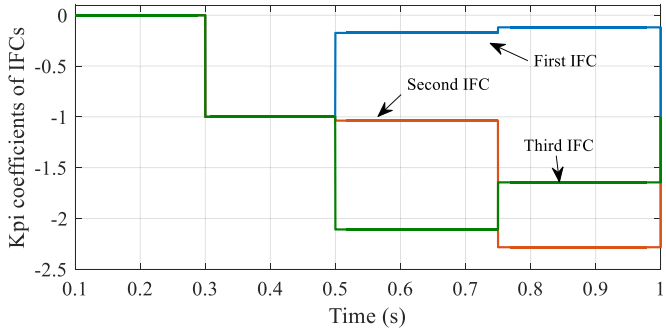

Fig. 6. Power coefficient factors in the control strategy-1.

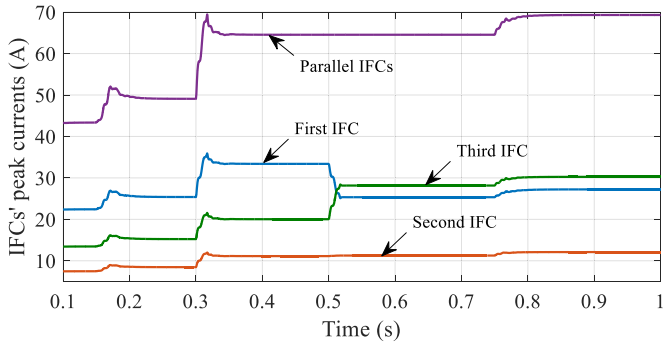

Fig. 7. Peak currents of IFCs in the control strategy-1.

mined. The determined k_{pi} of IFCs provide zero collective active power oscillation of parallel IFCs by (26), share collective peak current of parallel IFCs among them based on their power ratings by using (27) and (28), and assure maximum power/current transferring capability of parallel IFCs by (29). If determined k_{pi} from (26) to (28) are greater than zero, which lead IFCs' peak currents to different phases, they will be set to zero and the calculation will be repeated for the rest of IFCs to determine their k_{pi}. It is worth mentioning that the sharing factors in (28) are independent from the converters' operating points, and these factors provide the same available room for IFCs' operation. In this control strategy, since the control objectives are achieved by power coefficients' control, this control strategy is named as coefficient-based control strategy.

In Fig. 5, an example is provided to explain the proposed control strategy's performance in more detail. In this figure, the relationships between two-parallel IFCs' peak currents and k_{pi} under the same average active powers ($P_1 = P_2$) and different rating powers ($S_1 < S_2$) are shown, where the $I^{\max}_{pi} - k_{pi}$ relationships are assumed linear in their operation range (see Fig. 3). In the following, the concept of the proposed control strategy is explained by using this example.

1) The proposed control strategy initially sets k_{p1} and k_{p2} to -1 (point-1), where the active power oscillation of both IFCs are zero [(26) is satisfied]. At point-1, the collective peak current is not shared between IFCs based on their power ratings [(28) and (29) are not satisfied]. In other words, since $P_1 = P_2$ and $S_1 < S_2$, the second IFC's peak current's share should be higher than that of the first IFC's. Thus, the operating points of IFCs should change to decrease the first IFC's peak current and increase the second IFC's peak current (move toward point-2).
2) At point-2, it is assumed that the collective active power oscillation reaches zero again [(26) is satisfied]. Although the first IFC's peak current has been decreased and the second IFC's peak current has been increased, the peak currents sharing ratios should be checked. At this point, it is assumed that the collective peak current of parallel IFCs has not been shared between IFCs based on their power ratings [(28) and (29) are not satisfied]. Therefore, the search of operating point will be continued toward point-3.
3) If the operating point that satisfies (26)–(28) simultaneously cannot be achieved up to point-3, the k_{p1} will be set to zero, and the k_{p2} will be searched to satisfy (26). Although sharing of collective peak current among two-parallel IFCs has not been achieved in this case, all peak currents are in the same phase to maximize the power/current transferring capability.
4) In this control strategy, maximizing power/current transferring capability of parallel IFCs has higher priority. Thus, all k_{pi} should be $k_{pi} \leq 0$. Then, control strategy tries to share collective peak current among parallel IFCs based on their power ratings under $\Delta P = 0$. For example, at point-4, if all (26)–(28) are satisfied, the operating point will not be chosen since the summation of parallel IFCs' peak currents is not minimized ($I^{\max}_{p1-4} + I^{\max}_{p2-4} > I^{\max}_{p1-2} + I^{\max}_{p2-2}$).

As a numerical example, the proposed control strategy is applied into three-parallel IFCs, and the results are shown in Figs. 6–9. In this example, at $t = 0.15$ s, unbalance condition is applied. During $0.3 < t < 0.5$, collective power oscillation is kept zero by setting $k_{p1} = k_{p2} = k_{p3} = -1$ [see (26)]. However, the first IFC's current exceeds its rating limit ($I_1^{\text{rate}} = 30$ A), and the collective peak current is not shared among parallel IFCs based on their power ratings ($S_1 = 9$ kVA, $S_2 = 4$ kVA, $S_3 = 10$ kVA). Thus, at $t = 0.5$ s, the proposed control strategy is applied. At $t = 0.75$ s, average active powers of IFCs are modified from $P_1 = 6$ kW, $P_2 = 2$ kW, and $P_3 = 3.6$ kW to $P_1 = 6.5$ kW, $P_2 = 1.5$ kW, and $P_3 = 4.5$ kW. The results clarify that the collective active power oscillation

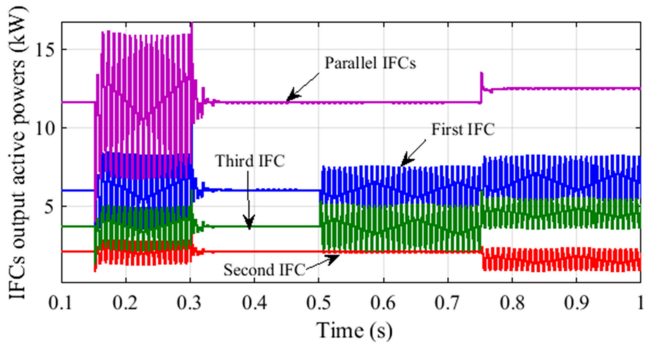

Fig. 8. Individual IFCs' output active powers and collective active power of parallel IFCs in the control strategy-1.

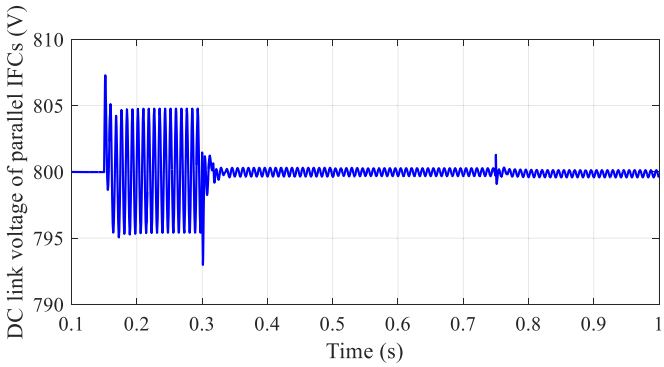

Fig. 9. DC-link voltage of parallel IFCs in the control strategy-1.

cancelation (oscillation-free dc-link voltage), collective peak current sharing, and maximum power transferring capability can be achieved by using (26)–(29).

In general, due to computational complexity in solving the set of nonlinear equations, the proposed control strategy's implementation can be complicated, and small calculation delay may be imposed. The proposed control strategy will not have errors in active power oscillation cancelation and collective peak current sharing among IFCs. However, under variation of IFCs' average active power flow directions and values, the power coefficients of IFCs should be recalculated and updated.

B. Control Strategy-2: Peak Current Based Control Strategy

To reduce the computational burden of the proposed control strategy-1, the peak current based control strategy is proposed here. This control strategy is based on the conclusion that has been achieved from (25). In the peak current based control strategy, following expressions are considered to achieve the control objectives:

$$I_{p1}^{\max} + I_{p2}^{\max} + \cdots + I_{pn}^{\max} \cong I_{p-\mathrm{IFCs}}^{\max}\big|_{\Delta P=0} \tag{30}$$

$$U_1 I_{p1}^{\max} = U_2 I_{p2}^{\max} = \cdots = U_n I_{pn}^{\max} \tag{31}$$

$$U_i = \frac{S_1}{S_i} \qquad i = 1,\ 2, \ldots, n \tag{32}$$

$$k_{pi} \le 0 \qquad i = 1,\ 2, \ldots, n \tag{33}$$

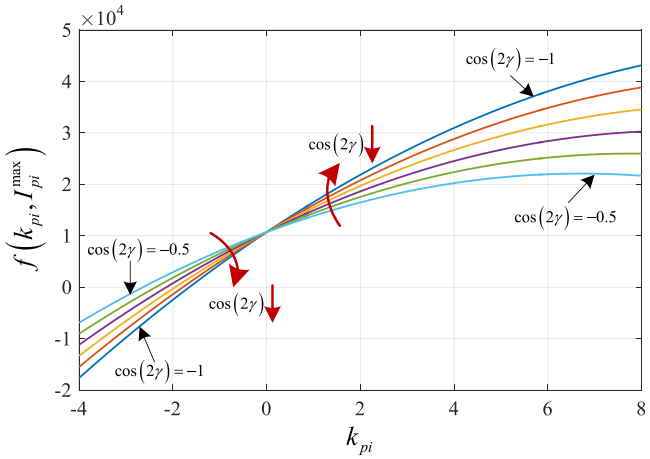

Fig. 10. Numerical example for $I_{pi}^{\max} - k_{pi}$ quadratic equation variations in (14) under fixed value of $I_{pi}^{\max} = 35$ A and different values of k_{pi} ($k_{pi}: -4 \rightarrow 8$) and γ ($\cos 2\gamma: -1 : 0.1 : -0.5$). ($|v^+| = 168$ V, $|v^-| = 16$ V, $P_i = 5$ kW).

where $I_{p-\mathrm{IFCs}}^{\max}\big|_{\Delta P=0}$ is obtained by using (18) and (19). In this control strategy, active power oscillation cancelation constraint is embedded in (30), and collective peak current sharing target is achieved by using (31) and (32). From (30) and (31), the $I_{pi}^{\max}$ for individual ith IFC under $\Delta P = 0$ can be calculated as follows:

$$I_{pi}^{\max} \cong \left(\frac{S_i}{S_1 + S_2 + \cdots + S_n}\right) \times I_{p-\mathrm{IFCs}}^{\max}\big|_{\Delta P=0}\ i = 1, \ldots, n. \tag{34}$$

After each IFC's reference peak current's calculation from (34), its k_{pi} can be determined by using (14) and (15). Similarly, the calculated k_{pi} of all IFCs should be less than zero to maximize the power/current transferring capability of parallel IFCs. It is worth mentioning that if $k_{pi} \le 0$, the minimum possible value of $I_{pi}^{\max}$ will be $P_i/|v^+|$ ($k_{pi} = 0$ in (14) and see Fig. 3), and if any calculated $I_{pi}^{\max}$ is less than $P_i/|v^+|$, it will be set to the limited value, and the calculation will be repeated for the rest of the IFCs. In this control strategy, since IFCs' peak currents are directly controlled, this control strategy is named as peak current based control strategy.

Considering (14), it can be concluded that if $P_i/|v^+| \le I_{pi}^{\max} \le P_i/|v^-|$, the $I_{pi}^{\max} - k_{pi}$ quadratic equation will have two different real roots for k_{pi} under determined value of $I_{pi}^{\max}$ and γ. These two roots have different signs. As mentioned, in this proposed control strategy, all IFCs' peak currents are controlled to be $I_{pi}^{\max} \ge P_i/|v^+|$. In addition, $I_{pi}^{\max} \le P_i/|v^-|$ is always satisfied since $|v^-|$ is small percentage of $|v^+|$ [30] and $P_i/|v^-|$ exceeds the current rating limit of IFC. As a result, $P_i/|v^+| \le I_{pi}^{\max} \le P_i/|v^-|$ is always satisfied. As an example, the $I_{pi}^{\max} - k_{pi}$ quadratic equation variations ($f(k_{pi}, I_{pi}^{\max})$) in (14) under fixed value of $I_{pi}^{\max}$ and different values of k_{pi} and γ are plotted in Fig. 10. As seen from the figure, for determined value of $I_{pi}^{\max}$, the $f(k_{pi}, I_{pi}^{\max})$ quadratic equation has two real roots for k_{pi} with different signs ($I_{pi}^{\max}$ is in the aforementioned boundary). In this figure, the roots with positive signs are not shown. From these discussions, it can be concluded that there is always a $k_{pi} < 0$ that satisfies the calculated $I_{pi}^{\max}$ from (34),

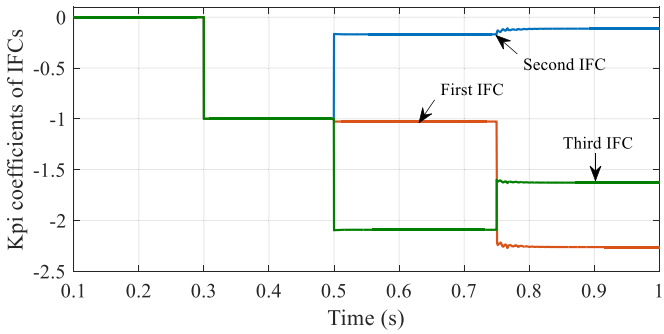

Fig. 11. Power coefficient factors in the control strategy-2.

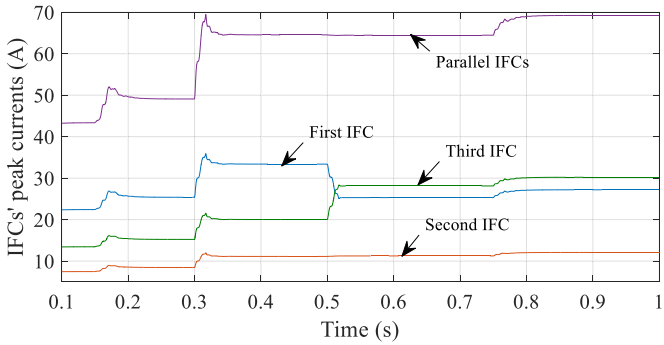

Fig. 12. Peak currents of IFCs in the control strategy-2.

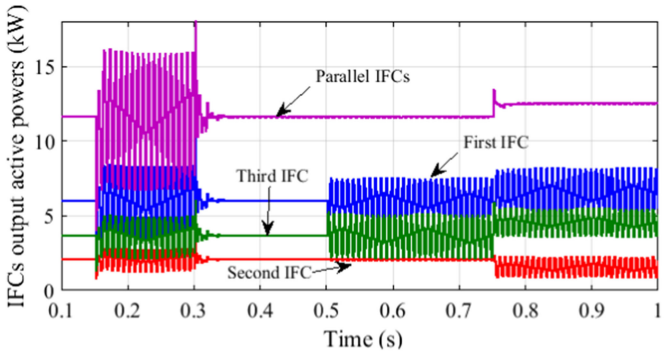

Fig. 13. Individual IFCs' output active powers and collective active power of parallel IFCs in the control strategy-2.

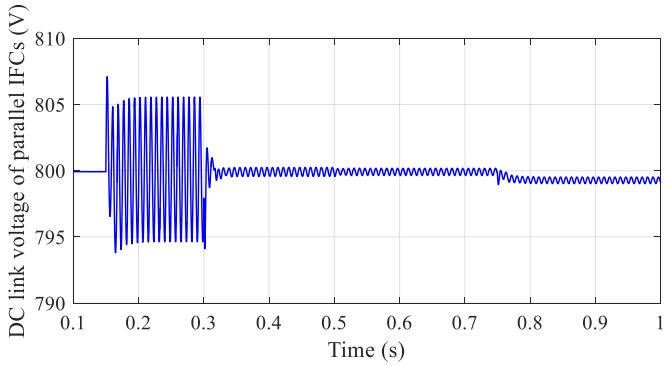

Fig. 14. DC-link voltage of parallel IFCs in the control strategy-2.

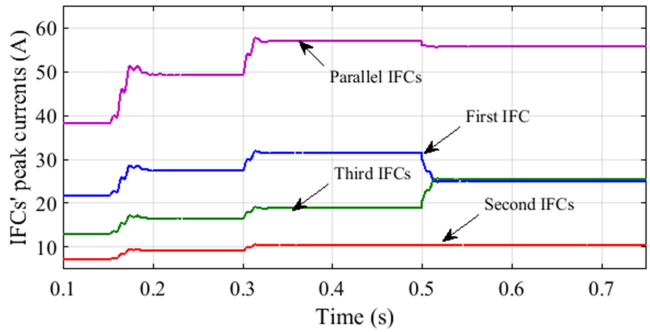

Fig. 15. Peak currents of IFCs in the control strategy-2 under $\mathrm{PF}_i = 0.7071$.

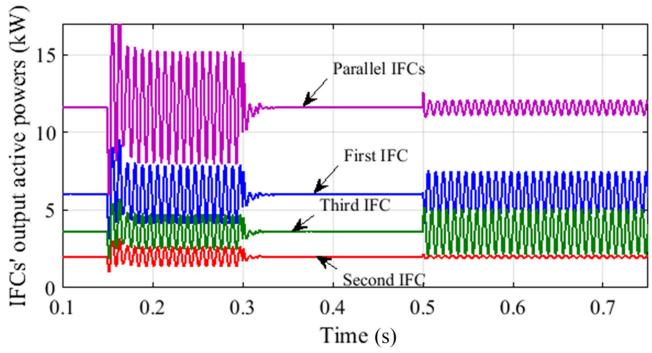

Fig. 16. Individual IFCs' output active powers and collective active power of parallel IFCs in the control strategy-2 under $\mathrm{PF}_i = 0.7071$.

which keeps the ith IFC's peak current in the same phase with collective peak current of parallel IFCs.

As a numerical example, and similar to the proposed control strategy-1, the proposed control strategy-2 is applied into three-parallel IFCs under unbalanced voltage, and the results are shown in Figs. 11 and 14 (test system is the same). Comparing these results with the results in Figs. 6 and 9 clarifies that the two proposed control strategies have similar performance.

As another example, the test is repeated; however, the IFCs' PFs are set to $\mathrm{PF}_i = 0.7071$ ($P_i = Q_i$) to evaluate the performance of the proposed control strategy under nonunity PFs. The results are shown in Figs. 15 and 16. From the results, it is concluded that the proposed control can reduce the active power oscillation of parallel IFCs by 90% (from $\Delta P_{\mathrm{peak-peak}} = 7.3$ kW to $\Delta P_{\mathrm{peak-peak}} = 0.8$ kW), and can provide peak current sharing among IFCs with high accuracy (maximum sharing error is 6%).

In general, the proposed control strategy-2 reduces the computational burden of active power oscillation cancelation and collective peak current sharing of parallel IFCs, and it can be implemented easily. Due to approximate calculations, the proposed control strategy may induce small errors. Similar to the proposed control strategy-1, individual IFCs' peak currents should be recalculated under variations of average active power flow directions and values.

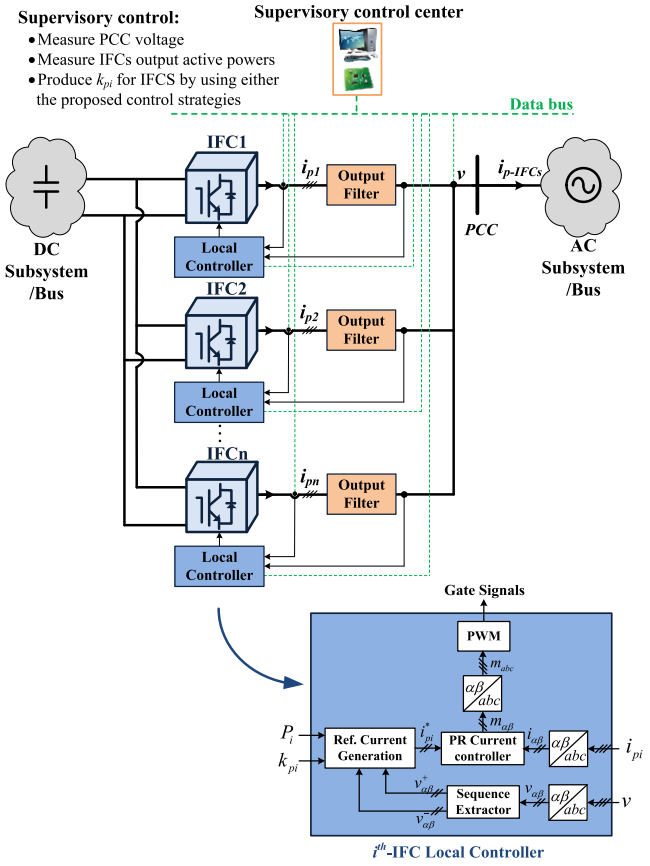

Fig. 17. General control structure of both the proposed control strategies.

Fig. 18. Photograph of experimental setup.

C. Proposed Control Strategies Implementation

In general, the two proposed control strategies are secondary controllers that have been designed to reduce the unbalanced voltage adverse effects on IFCs' operation in the steady-state condition. In detail, the three-phase voltage at the PCC as well as operating active powers of the IFCs are measured and sent to a supervisory control center. In the supervisory control, k_{pi} of all IFCs are calculated by using either the first or the second proposed control strategy. In the first control strategy, due to computational complexity in solving the set of nonlinear equations, implementation will be complicated and calculation delay may be imposed. Whereas in the second control strategy, computational burden has been reduced, and linear equations are solved to achieve k_{pi}. The calculated k_{pi} is transferred into local controllers of IFCs through low-bandwidth communication links. In Fig. 17, the general control structure of both the proposed control strategies is shown. It should be highlighted that the proposed control strategies are also applicable for IFCs not close to each other, considering the ongoing smart inverters' researches and projects where communication with central supervisory controller is their inevitable feature [31]–[33]. Moreover, due to computational burden reduction in the second proposed control strategy (only simple linear equations should be solved to calculate k_{pi}), this control strategy can be implemented in a master–slave control structure of closely located IFCs as well, where computations of all k_{pi} are done in a local controller of one of the IFCs (in one DSP) and sent to other IFCs' local controllers. Thus, a dedicated supervisory control is not necessary in this case.

In both the proposed control strategies, all parallel IFCs operate on power/current control mode in which the output currents of IFCs are controlled to regulate the output average powers on their reference values. The closed-loop current control in the stationary $\alpha\beta$ reference frame with practical proportional-resonant controller is used [34]. In the control strategies, frequency-locked loop-based sequence extractor in [35] is used to decompose the PCC voltage into positive and negative sequence components.

It should be highlighted that in the proposed strategies, the average active powers of IFCs are not changed by the control strategy. The real power reference can be determined from a separate control loop (such as MPPT in the PV system). In this paper, these parameters are considered as known values. Also, it is important to mention that both the proposed control strategies are applicable under different unbalanced voltage levels, even though larger available rooms of IFCs are necessary for higher unbalanced voltage levels.

V. Experimental Verification

Here, the effectiveness and performances of the proposed control strategies under different operating conditions are verified by experimental results. In the experimental tests, two-parallel three-phase IFCs are used. Here, the results of the second proposed control strategy, which can be implemented more easily in DSPs, are provided (it should be mentioned that both the proposed control strategies' performances are similar, further verifying the effectiveness of the second method that can be

TABLE I
SYSTEM PARAMETERS FOR EXPERIMENTS

	Symbol	Value
DC-link voltage	$v_{\rm dc}$	200 V
IFCs' power ratings	$S_i^{\rm rate}$	$S_1 = 1.25$ kVA; $S_2 = 1$ kVA
IFCs' output filters	L_f–C_f	3.6 mH – 4 μF
Switching frequency	f_s	10 kHz
Resistive load	R_L	5 Ω/phase

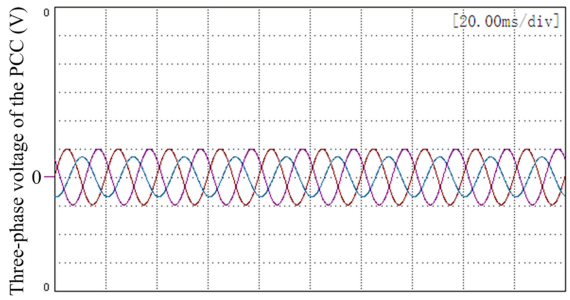

Fig. 19. Three-phase voltage of the PCC with 12% of the unbalanced level. v (100 V/div); (20 ms/div).

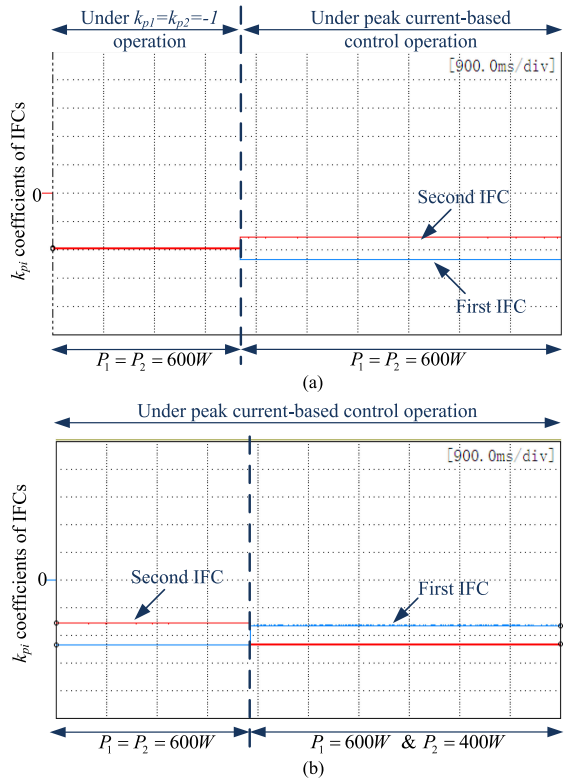

Fig. 20. k_{p1} and k_{p2} coefficient factors under (a) application of the proposed strategy, and (b) presence of the proposed strategy and variation of average active powers. k_{p1} (0.5/div) and k_{p2} (0.5/div); (900 ms/div).

implemented easily). In Fig. 18, the experimental setup photograph is shown, and the setup specifications are listed in Table I. In the setup, two DSPs with serial communication interface to realize communication system with the speed rate of 9600 b/s are used. Moreover, since the power flow of the ac source (the programmable ac source is used as the grid) is unidirectional,

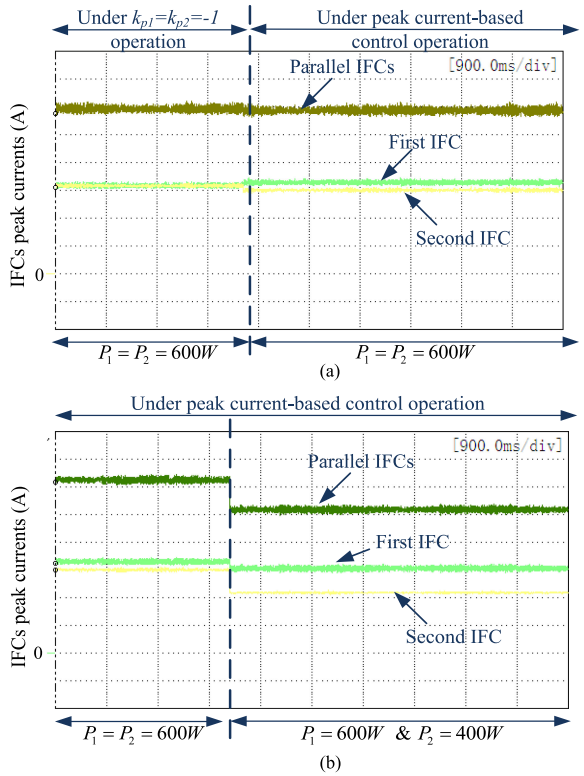

Fig. 21. Peak currents' of IFCs under (a) application of the proposed strategy and (b) presence of the proposed strategy and variation of average active powers. $I_{p-{\rm IFC}s}^{\max}$ (3 A/div), $I_{p1}^{\max}$ (3 A/div), and $I_{p2}^{\max}$ (3 A/div); (900 ms/div).

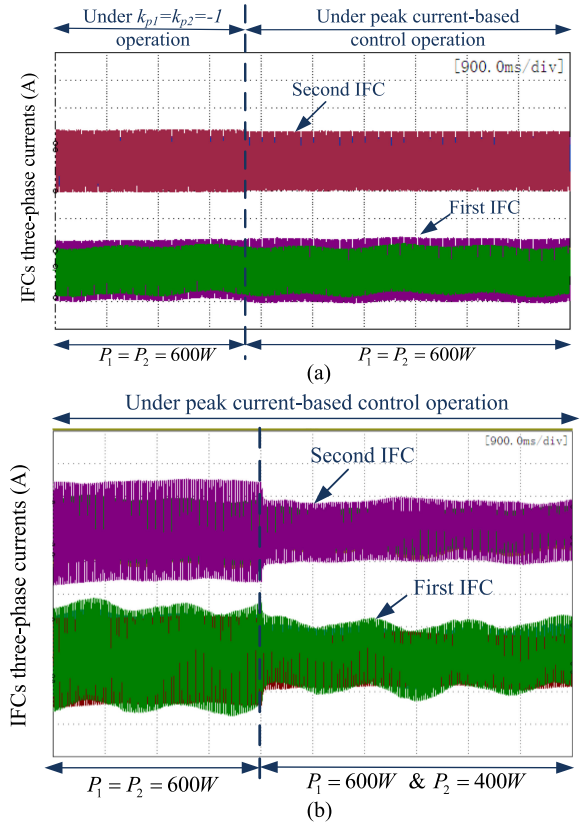

Fig. 22. First and second IFCs' instantaneous three-phase currents under (a) application of the proposed strategy, and (b) presence of the proposed strategy and variation of average active powers: i_{p1} (7 A/div) and i_{p2} (7 A/div); (900 ms/div).

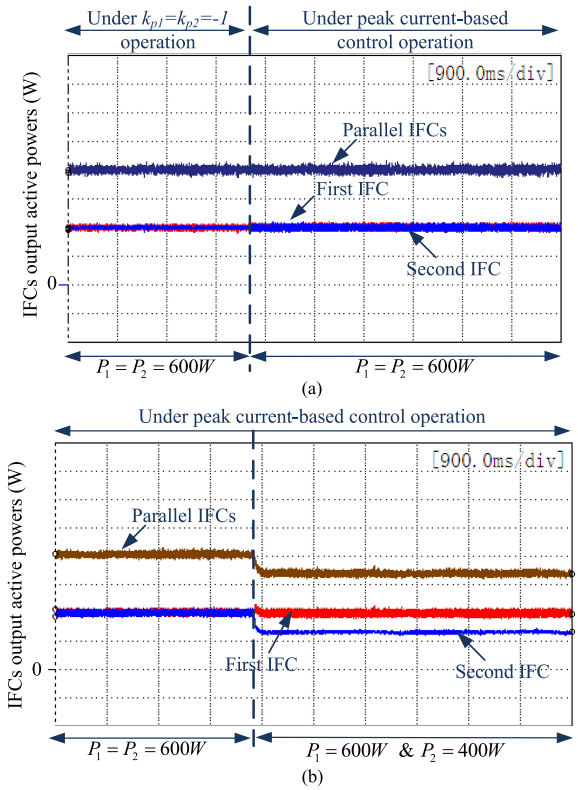

Fig. 23. Parallel IFCs collective active power, and first and second IFCs output active powers under (a) application of the proposed strategy, and (b) presence of the proposed strategy and variation of average active powers; p_1 (300W/div), p_2 (300W/div), and p(300W/div); (900ms/div).

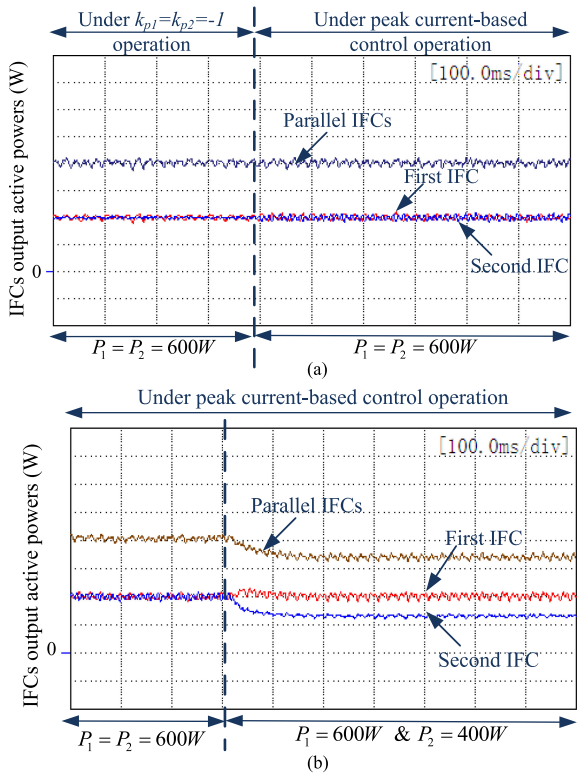

Fig. 24. Parallel IFCs collective active power, and first and second IFCs output active powers, zoomed-in view of the transition from (a) $k_{p1} = k_{p2} = -1$ operation into peak current-based control operation and (b) $P_1 = P_2 = 600$ W into $P_1 = 600$ W and $P_2 = 400$ W in the presence of the proposed strategy. p_1 (300 W/div), p_2 (300 W/div), and p(300 W/div); (100 ms/div).

three-phase resistive load is connected between the source and parallel converters at the PCC to absorb power from both ac source and converters.

In the experimental tests, the performance of the proposed control strategy under different unbalanced voltage levels and IFCs average active powers' variations are verified. For this purpose, two sets of tests are conducted under different unbalanced voltage levels in which the average active powers of the IFCs are varied in each set during the test.

A. *First Set of Tests: Unbalanced Voltage Level of* 12%

In the first set of tests, the three-phase voltages of the ac source are tuned on $v_a = 50\angle 0$, $v_b = 70\angle 245$, and $v_c = 70\angle 115$, which are shown in Fig. 19. At the beginning, the power coefficient factors are set to $k_{p1} = k_{p2} = -1$, which leads to zero active power oscillations of IFCs. Since the collective peak current of parallel IFCs is not shared between them based on their power ratings, the proposed control strategy is applied. Then, during the test, the IFCs' average active powers are modified from $P_1 = 600$ W and $P_2 = 600$ W to $P_1 = 600$ W and $P_2 = 400$ W.

The coefficient factor results are shown in Fig. 20. From the results, since coefficient factors are less than zero, the proposed control strategy provides maximum power/current transferring capability for parallel IFCs. The collective peak current of parallel IFCs and the first and second IFCs' peak currents are shown in Fig. 21. As clear from the figure, the parallel IFCs' collective peak current is constant under fixed average active powers of IFCs, which is decreased with the reduction of $\sum_{i=1}^{2} P_i$. Moreover, this current is shared between IFCs based on their power ratings after the proposed control strategy's application. In detail, since $S_1/S_2 \approx 5/4$, the first IFC provides higher portion of collective IFCs' peak current; $I_{p1}^{\max} \approx 5/4 \times I_{p2}^{\max}$. In Fig. 22, the first and second IFCs' instantaneous three-phase currents are shown, which verify the peak currents values of IFCs in Fig. 21. In Fig. 23, the collective active power of parallel IFCs and active powers of the first and second IFCs are shown.

As seen from the figure, after applying the proposed control strategy, the collective active power oscillation is similar to $k_{p1} = k_{p2} = -1$, and small oscillations are due to errors in voltage and current measurements. The zoomed-in view of the IFCs active powers during transition from $k_{p1} = k_{p2} = -1$ operation to peak current-based control operation, and from $P_1 = P_2 = 600$ W operation to $P_1 = 600$ W and $P_2 = 400$ W are shown in Fig. 24. Also, in Fig. 25, the zoomed-in view of the IFCs active powers during steady-state operation of the proposed control strategy under $P_1 = P_2 = 600$ W and $P_1 = 600$ W and $P_2 = 400$ W are depicted. As can be seen from Figs. 24 and 25, the power oscillations of the two IFCs are 180° out of phase to cancel out parallel IFCs power oscillations.

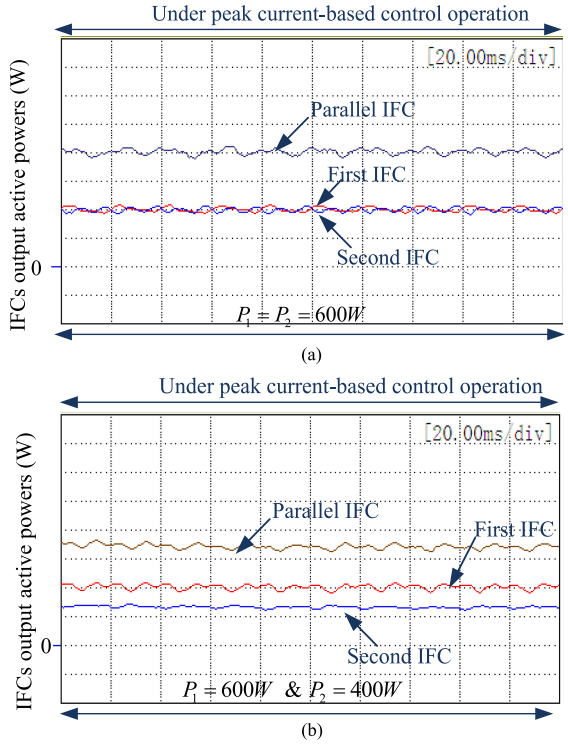

Fig. 25. Parallel IFCs collective active power, and first and second IFCs output active powers, zoomed in view of the steady-state operation of the proposed control strategy under (a) $P_1 = P_2 = 600$ W and (b) $P_1 = 600$ W and $P_2 = 400$ W. p_1 (300 W/div), p_2 (300 W/div), and p(300 W/div); (20 ms/div).

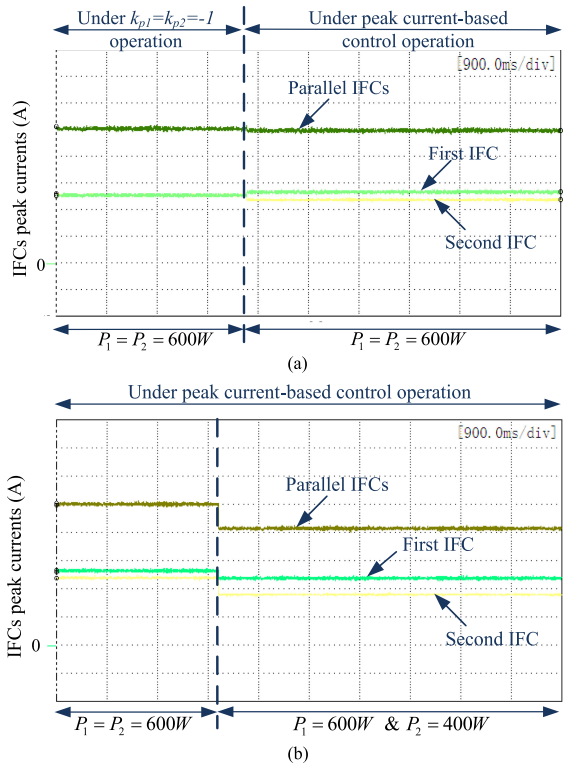

Fig. 27. Peak currents' of IFCs under (a) application of the proposed strategy, and (b) presence of the proposed strategy and variation of average active powers. $I_{p-\mathrm{IFC}s}^{\max}$ (3 A/div), $I_{p1}^{\max}$ (3 A/div), and $I_{p2}^{\max}$ (3 A/div); (900 ms/div).

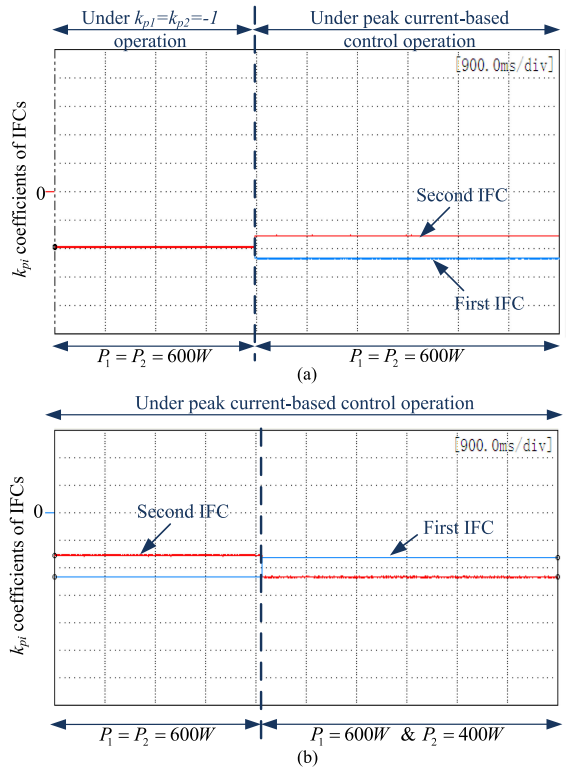

Fig. 26. k_{p1} and k_{p2} coefficient factors under (a) application of the proposed strategy, and (b) presence of the proposed strategy and variation of average active powers. k_{p1} (0.5/div) and k_{p2} (0.5/div); (90 ms/div).

B. *Second Set of Tests: Unbalanced Voltage Level of* 25%

Here, the proposed control strategy's performance under more severe unbalance condition is verified. As mentioned, the second set of tests is similar to the first one, and only the level of voltage unbalance is different. Here, the ac source three-phase voltages are adjusted to $v_a = 55\angle 0$, $v_b = 83.8\angle 250$, *and* $v_c = 83.8\angle 110$. In Fig. 26, the coefficient factor results are shown, which are less than zero that maximize the power/current transferring capability for parallel IFCs. The sharing of collective peak current of parallel IFCs between the first and second IFCs is shown in Fig. 27. It should be considered that the sharing factor is $5/4$ since $S_1/S_2 \approx 5/4$, similar to the first test. The first and second IFCs' active powers and collective active power of parallel IFCs are shown in Fig. 28. This figure shows that the collective active power oscillation after the proposed control application is similar to $k_{p1} = k_{p2} = -1$ operation.

Finally, considering the experimental results in Figs. 20–28 clarifies that in the proposed control strategies, the following statements hold.

1) All IFCs' peak currents are kept in the same phase with collective peak current of parallel IFCs (power/current transferring capability is maximized).

2) Collective peak current is shared among parallel IFCs based on their power ratings.

3) Active power oscillations are collectively canceled out (provides oscillation-free dc link).

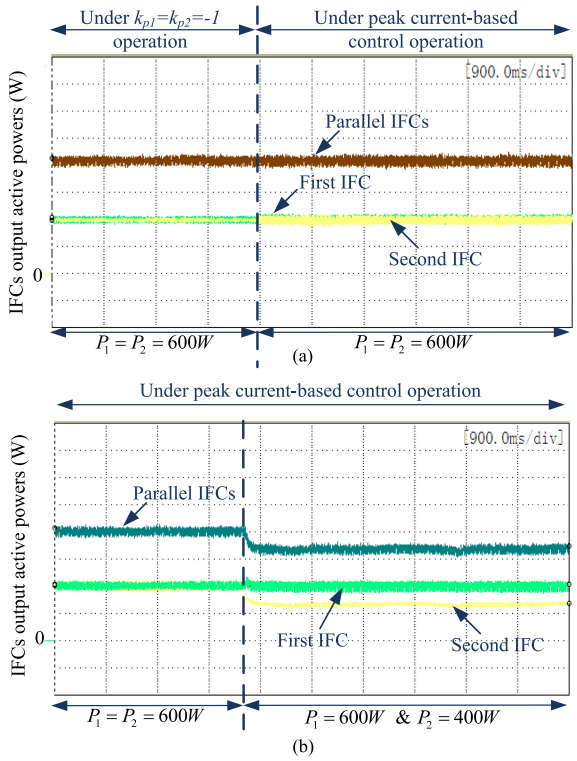

Fig. 28. Parallel IFCs' collective active power, and the first and second IFCs output active powers under (a) application of the proposed strategy, and (b) presence of the proposed strategy and variation of average active powers. p_1 (300 W/div), p_2 (300 W/div), and p(300 W/div); (900 ms/div).

VI. Conclusion

In this paper, two control strategies for parallel power electronics IFCs under unbalanced voltage are proposed, where they improve the power quality in both ac and dc sides of hybrid ac/dc microgrids. The both proposed strategies are secondary controllers that have been designed to operate in the steady-state condition. The proposed control strategies cancel out active power oscillations of parallel IFCs, control IFCs' peak currents based on their power ratings, and minimize the peak current of parallel IFCs. In the first proposed strategy, power coefficients of IFCs are controlled. Due to computational complexity in solving the set of nonlinear equations, implementation will be complicated. In the second proposed control strategy, computational burden has been reduced, and peak currents of IFCs are directly controlled through the derived linear relationship of IFCs' peak currents under zero power oscillation. In this paper, thorough study on parallel IFCs power/current transferring capability is conducted. It is proven that collective peak current of parallel IFCs is a constant value under zero active power oscillations and fixed average active powers, and power/current transferring capability of parallel IFCs is maximized when peak currents of all individual IFCs and collective peak current of parallel IFCs are in the same phase and in-phase. The numerical examples and experimental results are provided to verify the analysis and two proposed control strategies in this paper.

References

[1] F. Nejabatkhah and Y. W. Li, "Overview of power management strategies of hybrid AC/DC microgrid," *IEEE Trans. Power. Electron.*, vol. 30, no. 12, pp. 7072–7089, Dec. 2015.

[2] A. Von Jouanne and B. Banerjee, "Assessment of voltage unbalance," *IEEE Trans. Power Del.*, vol. 16, no. 4, pp. 782–790, Oct. 2001.

[3] L. Tzung-Lin, H. Shang-Hung, and C. Yu-Hung, "D-STATCOM with positive-sequence admittance and negative-sequence conductance to mitigate voltage fluctuations in high-level penetration of distributed-generation systems," *IEEE Trans. Ind. Electron.*, vol. 60, no. 4, pp. 1417–1428, Apr. 2013.

[4] M. Savaghebi, A. Jalilian, J. C. Vasquez, and J. M. Guerrero, "Autonomous voltage unbalance compensation in an islanded droop-controlled microgrid," *IEEE Trans. Ind. Electron.*, vol. 60, no. 4, pp. 1390–1402, Apr. 2013.

[5] N. Femia, G. Petrone, G. Spagnuolo, and M. Vitelli, "Optimization of perturb and observe maximum power point tracking method," *IEEE Trans. Power Electron.*, vol. 20, no. 4, pp. 963–973, Jul. 2005.

[6] N. Femia, G. Petrone, G. Spagnuolo, and M. Vitelli, "A new analog MPPT technique: Teodi," *Prog. Photovolt. Res. Appl.*, vol. 18, no. 1, pp. 28–41, 2010.

[7] D. G. Montoya, C. A. Ramos-Paja, and R. Giral, "Improved design of sliding-mode controllers based on the requirements of MPPT techniques," *IEEE Trans. Power Electron.*, vol. 31, no. 1, pp. 235–247, Jan. 2016.

[8] F. Nejabatkhah, Y. W. Li, and B. Wu, "Control strategies of three-phase distributed generation inverters for grid unbalanced voltage compensation," *IEEE Trans. Power. Electron.*, vol. 31, no. 7, pp. 5228–5241, Jul. 2016.

[9] A. Camacho, M. Castilla, J. Miret, A. Borrell, and L. de Vicuna, "Active and reactive power strategies with peak current limitation for distributed generation inverters during unbalanced grid faults," *IEEE Trans. Ind. Electron.*, vol. 62, no. 3, pp. 1515–1525, Mar. 2015.

[10] F. Wang, J. L. Duarte, and M. A. M. Hendrix, "Pliant active and reactive power control for grid-interactive converters under unbalanced voltage dips," *IEEE Trans. Power Electron.*, vol. 26, no. 5, pp. 1511–1521, May 2011.

[11] J. Lu, F. Nejabatkhah, Y. Li, and B. Wu, "DG control strategies for grid voltage unbalance compensation," in *Proc. IEEE Energy Convers. Congr. Expo.*, 2014, pp. 2932–2939.

[12] S. Chaudhary, R. Teodorescu, P. Rodriguez, P. Kjaer, and A. Gole, "Negative sequence current control in wind power plants with VSCHVDC connection," *IEEE Trans. Sustain. Energy*, vol. 3, no. 3, pp. 535–544, Jul. 2012.

[13] V. Valouch, M. Bejvl, P. Simek, and J. Skramlik, "Power control of grid-connected converters under unbalanced voltage conditions," *IEEE Trans. Ind. Electron.*, vol. 62, no. 7, pp. 4241–4248, Jul. 2015.

[14] M. Hamouda, H. F. Blanchette, and K. Al-Haddad, "Unity power factor operation of indirect matrix converter tied to unbalanced grid," *IEEE Trans. Power Electron.*, vol. 31, no. 2, pp. 1095–1107, Feb. 2016.

[15] J. Miret, M. Castilla, A. Camacho, L. G. de Vicua, and J. Matas, "Control scheme for photovoltaic three-phase inverters to minimize peak currents during unbalanced grid-voltage sags," *IEEE Trans. Power Electron.*, vol. 27, no. 10, pp. 4262–4271, Oct. 2012.

[16] C. T. Lee, C. W. Hsu, and P. T. Cheng, "A low-voltage ride-through technique for grid-connected converters of distributed energy resources," *IEEE Trans. Ind. Appl.*, vol. 47, no. 4, pp. 1821–1832, Jul. 2011.

[17] M. Savaghebi, A. Jalilian, J. C. Vasquez, and J. M. Guerrero, "Autonomous voltage unbalance compensation in an islanded droop-controlled microgrid," *IEEE Trans. Ind. Electron.*, vol. 60, no. 4, pp. 1390–1402, Apr. 2013.

[18] M. Hamzeh, H. Karimi, and H. Mokhtari, "A new control strategy for a multi-bus MV microgrid under unbalanced conditions," *IEEE Trans. Power Sys.*, vol. 27, no. 4, pp. 2225–2233, Nov. 2012.

[19] P. T. Cheng, C. Chen, T. L. Lee, and S. Y. Kuo, "A cooperative imbalance compensation method for distributed-generation interface converters," *IEEE Trans. Ind. Appl.*, vol. 45, no. 2, pp. 805–815, Mar./Apr. 2009.

[20] D. De and V. Ramanarayanan, "Decentralized parallel operation of inverters sharing unbalanced and non-linear loads," *IEEE Trans. Power Electron.*, vol. 25, no. 12, pp. 3015–3025, Aug. 2010.

[21] L. Meng, F. Tang, M. Savaghebi, J. C. Vasquez, and J. M. Guerrero, "Tertiary control of voltage unbalance compensation for optimal power quality in islanded microgrids," *IEEE Trans. Energy Convers.*, vol. 29, no. 4, pp. 802–816, Dec. 2014.

[22] E. Rezaei and S. Afsharnia, "Cooperative voltage balancing in islanded microgrid with single-phase loads," in *Proc. Elect. Control Eng. Conf.*, 2011, pp. 5804–5808.
[23] M. Savaghebi, A. Jalilian, J. C. Vasquez, and J. M. Guerrero, "Secondary control scheme for voltage unbalance compensation in an islanded droop-controlled microgrid," *IEEE Trans. Smart Grid*, vol. 3, no. 2, pp. 797–808, Jun. 2012.
[24] X. Hu, X. Tang, N. Li and G. Zhang, "Virtual impedance based parallel operation of multi-converters in low voltage microgrids," in *Proc. Instrum. Meas. Sensor Netw. Autom. Conf.*, 2013, pp. 1031–1036.
[25] F. Wang, H. Mao, D. Xu, and Y. Ruan, "Negative-sequence admittance control scheme for distributed compensation of grid voltage unbalance," in *Proc. IEEE 13th Workshop Control Model. Power Electron.*, 2012, pp. 1–8.
[26] K. Sun, X. Wang, Y. W. Li, F. Nejabatkhah, Y. Mei, and X. Lu, "Parallel operation of bi-directional interfacing converters in a hybrid AC/DC microgrid under unbalanced grid voltage conditions," *IEEE Trans. Power. Electron.*, vol. 32, no. 3, pp. 1872–1884, Mar. 2017.
[27] F. Nejabatkhah, Y. Li, and K. Sun, "Parallel three-phase interfacing converters operation under unbalanced voltage in hybrid AC/DC microgrid," *IEEE Trans. Smart Grid*, to be published.
[28] F. Nejabatkhah, Y. Li, and K. Sun, "Peak current-based control of parallel three-phase interfacing converters operation under unbalanced voltage," in *Proc. IEEE 8th Int. Power Electron. Motion Control Conf.*, Hefei, 2016, pp. 157–162.
[29] R. Teodorescu, M. Liserre, and P. Rodrıguez, *Grid Converters for Photovoltaic and Wind Power Systems*. New York, NY, USA: Wiley, 2011.
[30] *IEEE Recommended Practice for Monitoring Electric Power Quality*, IEEE Std 1159-2009 (Revision of IEEE Std 1159-1995), Jun. 2009.
[31] R. Edge, B. York, and N. Enbar, "Rolling out smart inverters: Assessing utility strategies and approaches," *Sol. Elect. Power Assoc.*, Washington, DC, USA, Technical Results, 2015.
[32] Electric Power Research Institute, "Common functions for smart inverters: 4th Edition," Elect. Power Res. Inst., Palo Alto, CA, USA, 2016.
[33] Pinnacle West Capital Corporation, "2014 annual report," Pinnacle West Capital Corporation, Phoenix, AZ, USA, 2014. [Online]. Available: http://www.azenergyfuture.com/getmedia/d2202ba5-41aa-4ef2-b8c1-411d2f074654/PNW_2014_Annual_Report.pdf/?ext=.pdf
[34] A. Vidal *et al.*, "Assessment and optimization of the transient response of proportional-resonant current controllers for distributed power generation systems," *IEEE Trans. Ind. Electron.*, vol. 60, no. 4, pp. 1367–1383, Apr. 2013.
[35] P. Rodriguez, A. Luna, I. Candela, R. Mujal, R. Teodorescu, and F. Blaabjerg, "Multiresonant frequency-locked loop for grid synchronization of power converters under distorted grid conditions," *IEEE Trans. Ind. Electron.*, vol. 58, no. 1, pp. 127–138, Jan. 2011.

Farzam Nejabatkhah (S'09) received the B.Sc. (Hons.) and M.Sc. (Hons.) degrees in electrical engineering from the University of Tabriz, Tabriz, Iran, in 2009 and 2011, respectively, and the Ph.D. degree in electrical engineering-energy system from the University of Alberta, Edmonton, AB, Canada, in 2017.

Since then, he has been a Postdoctoral Research Fellow with the University of Alberta. His research interests include hybrid ac/dc microgrids, smart grids, power quality control, renewable energy and distributed generation, and power converter topologies and control.

Yun Wei Li (S'04–M'05–SM'11) received the B.Sc. degree in electrical engineering from the Tianjin University, Tianjin, China, in 2002, and the Ph.D. degree in electrical engineering from the Nanyang Technological University, Singapore, in 2006.

In 2005, he was a Visiting Scholar with the Aalborg University, Aalborg, Denmark. From 2006 to 2007, he was a Postdoctoral Research Fellow with the Ryerson University, Toronto, ON, Canada. In 2007, he also worked with Rockwell Automation, Prince George, BC, Canada, before he joined the University of Alberta in the same year. Since then, he has been with the University of Alberta, Edmonton, AB, Canada, where he is currently a Professor. His research interests include distributed generation, microgrid, renewable energy, high-power converters, and electric motor drives.

Dr. Li serves as an Associate Editor for the IEEE TRANSACTIONS ON POWER ELECTRONICS, the IEEE TRANSACTIONS ON INDUSTRIAL ELECTRONICS, the IEEE TRANSACTIONS ON SMART GRID, and the IEEE JOURNAL OF EMERGING AND SELECTED TOPICS IN POWER ELECTRONICS. He is the recipient of the Richard M. Bass Outstanding Young Power Electronics Engineer Award from the IEEE Power Electronics Society in 2013 and the Second Prize Paper Award of the IEEE TRANSACTIONS ON POWER ELECTRONICS in 2014.

Kai Sun (M'12–SM'16) received the B.E., M.E., and Ph.D. degrees in electrical engineering from the Tsinghua University, Beijing, China, in 2000, 2002, and 2006, respectively.

He joined the Faculty of Electrical Engineering, Tsinghua University, in 2006, where he is currently an Associate Professor. From September 2009 to August 2010, he was a Visiting Scholar with the Department of Energy Technology, Aalborg University, Aalborg, Denmark. From January to August 2017, he was a Visiting Professor with the Department of Electrical and Computer Engineering, University of Alberta, Edmonton, AB, Canada. His research interests include power electronics for renewable generation systems, microgrids, and energy internet.

Dr. Sun is a Member of the IEEE Power Electronics Society Sustainable Energy Systems Technical Committee, a Member of the IEEE Power Electronics Society Power and Control Core Technologies Committee, and a Member of the IEEE Industrial Electronics Society Renewable Energy Systems Technical Committee. He serves as an Associate Editor for the IEEE TRANSACTIONS ON POWER ELECTRONICS, the IEEE JOURNAL OF EMERGING AND SELECTED TOPICS IN POWER ELECTRONICS, and *Journal of Power Electronics*. He served as the TPC Vice Chair of IEEE ECCE2017 and IEEE ECCE-Asia2017. He was the recipient of the Delta Young Scholar Award in 2013 and the Youth Award of China Power Supply Society in 2017.

Ruixue Zhang was born in China in 1993. She received the B.E. degree in electrical engineering and automation from the Luoyang Normal University, Luoyang, China, in 2015, and the Master's degree from the Xi'an University of Technology, Xi'an, China, in 2015, and majored in electrical engineering.

She is currently a Joint Training Student with the Tsinghua University, Beijing, China. Her research interests include virtual synchronous generator and grid-connected inverters.